

Conformational Preferences of a 14-Residue Fibrillogenic Peptide from Acetylcholinesterase[†]

Ranjit Vijayan and Philip C. Biggin*

Department of Biochemistry, University of Oxford, Oxford OX1 3QU, United Kingdom

Received September 15, 2009; Revised Manuscript Received March 8, 2010

ABSTRACT: A 14-residue fragment from near the C-terminus of the enzyme acetylcholinesterase (AChE) is believed to have a neurotoxic/neurotrophic effect acting via an unknown pathway. While the peptide is α -helical in the full-length enzyme, the structure and association mechanism of the fragment are unknown. Using multiple molecular dynamics simulations, starting from a tetrameric complex of the association domain of AChE and systematically disassembled subsets that include the peptide fragment, we show that the fragment is incapable of retaining its helicity in solution. Extensive replica exchange Monte Carlo folding and unfolding simulations in implicit solvent with capped and uncapped termini failed to converge to any consistent cluster of structures, suggesting that the fragment remains largely unstructured in solution under the conditions considered. Furthermore, extended molecular dynamics simulations of two steric zipper models show that the peptide is likely to form a zipper with antiparallel sheets and that peptides with mutations known to prevent fibril formation likely do so by interfering with this packing. The results demonstrate how the local environment of a peptide can stabilize a particular conformation.

In cholinergic synapses and neuromuscular junctions, the enzyme acetylcholinesterase (AChE)¹ rapidly hydrolyzes the neurotransmitter acetylcholine, thereby terminating signal transmission (1). However, recent studies have shown that a 14-residue (AEFHRWSSYMVHWK) peptide fragment from the C-terminal tetramerization domain of the T-form of AChE has a deleterious effect on neurons acting via a yet to be confirmed pathway (2–7). While the peptide is helical in the tetramerization domain of AChE, the precise structure of the isolated peptide or the aggregated complex is currently unknown. Since this peptide has been likened to the amyloidogenic A β peptide implicated in Alzheimer's disease (3, 8, 9), it is of benefit to study its conformational stability and fibrillogenic propensity. Molecular modeling simulations could be used to provide insights into the conformational changes of the peptide in various states.

Crystal structures of the catalytic domain of AChE do not include the association domain (Figure S1 of the Supporting Information) where the peptide fragment resides since they were grown from truncated enzymes lacking this region. However, there is an X-ray crystal structure [Protein Data Bank (PDB) entry 1VZJ] of the isolated tetrameric C-terminal association domain of AChE in complex with a proline-rich attachment domain (PRAD) of the protein ColQ (Figure 1A) (10). The residues in the five chains of the crystal structure are shown in Figure 1B. In the wild-type protein complex, AChE and ColQ associate with a series of intra- and intermolecular disulfide bridges. However, these disulfide bridges are not essential for the

maintenance of the quaternary structure of the complex and are not included in the X-ray structures (10).

The peptide fragment has an α -helical conformation in each of the four subunits (chains I–IV in Figure 1A). However, this fragment has been shown to exist in alternate states. Using conformation-sensitive monoclonal antibodies, this fragment has been shown to exist as a β -strand (11). Furthermore, using the hidden β -propensity method, this region has been predicted to have a high β -sheet propensity (4). Such α -helix to β -sheet transition is a characteristic of many fibrillogenic peptides (12, 13).

To assess the stability of the peptide in the tetramer and the unfolding pathway of the peptide, the associated attachment domain, we performed multiple long molecular dynamics simulations of the protein in water. First, the intact tetramer with the PRAD domain was simulated (Figure 1A). In another set of simulations, the central PRAD helix was removed and the AChE tetrameric assembly (Figure 1C) was simulated to study its conformational stability in the absence of PRAD. To study the behavior of a monomer in isolation, a single helix (Figure 1D) from the four-helix bundle was simulated. Finally, we extracted the 14-residue AChE peptide from a helix (Figure 1E) and performed simulations, totaling 1.1 μ s, to determine its conformational preferences in a solvent modeled explicitly.

Numerous computer simulation studies, some at a very large scale (14), have looked at the protein folding problem (15). Most biologically relevant peptides fold on time scales not normally accessible through conventional MD simulations. Insufficient sampling and kinetic trapping often restrict the conformations accessible through such simulations. The replica exchange method (16), where multiple copies of a peptide are simulated at a range of temperatures and swapped at regular intervals based on a Metropolis criterion, is often used in peptide folding studies to overcome some of these pitfalls. Quite often, implicit solvent models (17) are also employed to significantly reduce the

[†]This work was supported by the Wellcome Trust. P.C.B. is a Research Councils UK fellow.

*To whom correspondence should be addressed. E-mail: philip.biggin@bi.ox.ac.uk. Phone: +44 1865 613305. Fax: +44 1865 613238.

¹Abbreviations: AChE, acetylcholinesterase; AChE peptide, 14-residue peptide from acetylcholinesterase; MC, Monte Carlo; MD, molecular dynamics; PRAD, proline-rich attachment domain; REMC, replica exchange Monte Carlo.

computational effort that would otherwise have been spent on computing the dynamics of the vast number of water molecules (18). To further explore the conformations sampled by the AChE peptide in solution, replica exchange Monte Carlo simulations were performed. Such simulations, ideally suited for small

peptides, have been reported to produce results in agreement with experimental data (19–24).

The isolated solution state structure of a peptide need not necessarily be the same as the aggregated state. Fibrillogenic peptides aggregate over long time scales ranging from minutes to days (25). These fibrils have been grouped into distinct classes of steric zippers on the basis of how individual peptide chains are oriented in a sheet and between adjacent sheets (26). It has been suggested that the AChE peptide could aggregate as a class 1 or class 5 steric zipper (4). In a class 1 zipper, the strands are arranged parallel in sheets and sheets are antiparallel, whereas in a class 5 zipper, the strands are arranged antiparallel in sheets and sheets are antiparallel. Here models of both classes were studied to elucidate the behavior of the peptide in the two plausible assemblies. Furthermore, the behavior of two mutants, W6A and M10A, known to prevent fibril formation (4) was also studied. Since pH has an impact on aggregation, to mimic such variations, steric zipper models with protonated histidines were also simulated.

In this work, using MD and REMC simulations, we show that under different conditions the AChE peptide is capable of existing in multiple states: α -helix, random coil, and β -sheet. Furthermore, we show that the mutations and pH could have an effect on the ability of the peptide to form conformationally stable fibril assemblies.

METHODS

Molecular Dynamics. Chains E–H (numbered I–IV, respectively) of the tetrameric AChE C-terminal region and chain J (numbered V) of the proline-rich attachment domain (PRAD) of the ColQ protein (Figure 1A) were extracted from the crystal structure (PDB entry 1VZJ). In simulations, the selenomethionines in the X-ray structure were replaced with methionines. The residues in the five chains are shown in Figure 1B. Four sets of simulations, with two repeats, were performed as listed in Table 1. The GROMACS 3.3.3 (27, 28) simulation package was used for all simulations. Protein atoms were described using the all-atom OPLS-AA force field (29, 30) since it has been shown to reproduce NMR data in folding simulations of amyloidogenic peptides (31). The TIP3P water model (32) was used. For simulations involving the AChE tetramer, the protein was solvated in a 150 mM NaCl box ($70 \text{ \AA} \times 70 \text{ \AA} \times 70 \text{ \AA}$). A larger box ($90 \text{ \AA} \times 90 \text{ \AA} \times 90 \text{ \AA}$) was used for the AChE monomer simulations to accommodate any likely unfolding, and a smaller box ($60 \text{ \AA} \times 60 \text{ \AA} \times 60 \text{ \AA}$) was used for the 14-residue peptide simulations. Periodic boundary conditions were enforced.

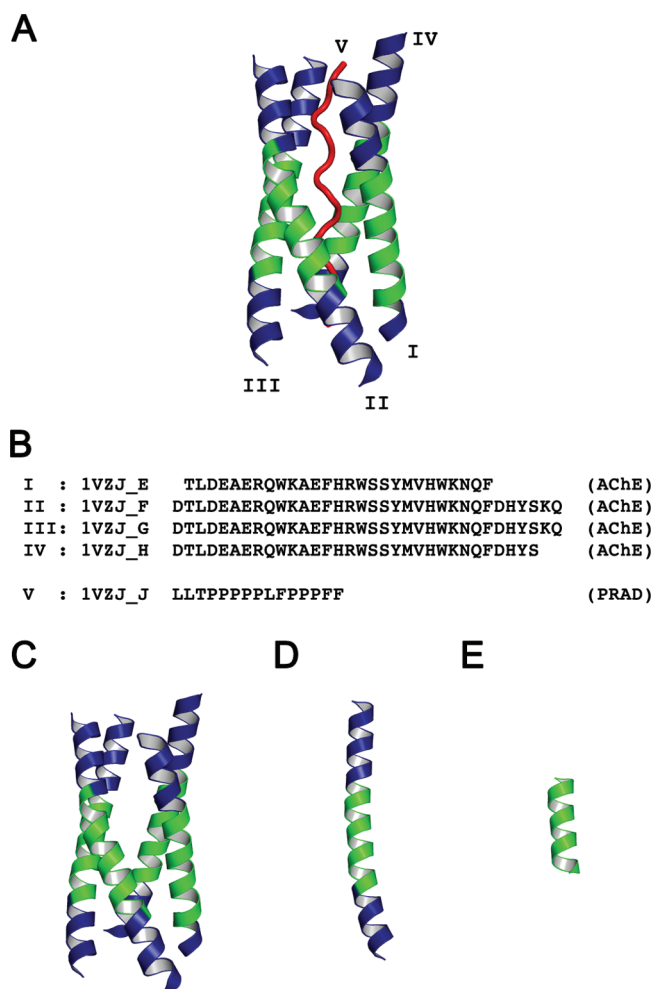


FIGURE 1: (A) AChE–PRAD complex with four AChE helices (blue and green) coiled around an antiparallel PRAD helix (red) (PDB entry 1VZJ). (B) Sequence of chains E–H and J from the structure. I–V is the numbering used in panel A to denote protein chains. (C) Four AChE helices without the PRAD helix. (D) One AChE helix. (E) Fourteen-residue AChE peptide extracted from an AChE monomer (highlighted in green throughout).

Table 1: MD Simulation of the AChE Peptide^a

simulation	simulation name	time (ns)	description
1	[AChE] ₄ -PRAD-1 (Figure 1A)	100	AChE tetramer and PRAD, run 1
2	[AChE] ₄ -PRAD-2 (Figure 1A)	75	AChE tetramer and PRAD, run 2
3	[AChE] ₄ -PRAD-3 (Figure 1A)	50	AChE tetramer and PRAD, run 3
4	[AChE] ₄ -1 (Figure 1C)	100	AChE tetramer without PRAD, run 1
5	[AChE] ₄ -2 (Figure 1C)	75	AChE tetramer without PRAD, run 2
6	[AChE] ₄ -3 (Figure 1C)	50	AChE tetramer without PRAD, run 3
7	[AChE] ₁ -1 (Figure 1D)	100	one chain (chain II) of AChE, run 1
8	[AChE] ₁ -2 (Figure 1D)	75	one chain (chain II) of AChE, run 2
9	[AChE] ₁ -3 (Figure 1D)	50	one chain (chain II) of AChE, run 3
10	peptide-1 (Figure 1E)	500	14-residue AChE peptide, run 1
11	peptide-2 (Figure 1E)	300	14-residue AChE peptide, run 2
12	peptide-3 (Figure 1E)	300	14-residue AChE peptide, run 3

^aIn each case, simulations were started with the corresponding segment extracted from the crystal structure (PDB entry 1VZJ).

Table 2: Replica Exchange Monte Carlo Folding–Unfolding Simulations

simulation	simulation name	MC steps (billion)	description
1	PEP-EXT-UNCAP	5	14-residue AChE peptide with charged termini started from an extended conformation
2	PEP-HEL-UNCAP	5	14-residue AChE peptide with charged termini started from the crystal structure (PDB entry 1VZJ)
3	PEP-EXT-CAP	5	14-residue AChE peptide with acetylated and amidated termini started from an extended conformation
4	PEP-HEL-CAP	5	14-residue AChE peptide with acetylated and amidated termini started from the crystal structure (PDB entry 1VZJ)

Langevin dynamics simulations were performed at 300 K using a stochastic dynamics integrator (33). A pressure of 1 bar was maintained (34). A 2 fs time step was used. Bonds involving hydrogen atoms were constrained using LINCS (35). The particle mesh Ewald method was used to handle long-range electrostatics with a real space cutoff of 10 Å. van der Waals interactions were switched off smoothly between 8 and 9 Å. Long-range dispersion correction was applied to energy and pressure to compensate for truncation effects.

The simulation protocol consisted of energy minimization of the system using the steepest descent algorithm followed by a 200 ps run where the heavy atoms were restrained using a harmonic potential with a force constant of 1000 kJ mol⁻¹ nm⁻² in the three spatial dimensions. Production simulations were run after the restraints were removed.

The secondary structure of the protein was determined using DSSP (36).

Replica Exchange Molecular Dynamics (REMC). All REMC simulations were performed using an efficient concerted rotation Monte Carlo sampling algorithm (19) implemented in HIPPO (<http://www.biowerkzeug.org>). To enhance sampling, an implicit solvent model was adopted (37). The OPLS-AA force field was used to describe the protein. Table 2 provides a list of simulations performed. In all cases, 12 replicas were used with temperatures of 275, 290, 307, 324, 342, 361, 381, 402, 425, 449, 474, and 500 K. REMC simulations were performed starting from an extended conformation of the 14-residue AChE peptide as well as the helical structure (Figure 1E) extracted from the crystal structure (PDB entry 1VZJ). It has been suggested that implicit solvent models overstabilize salt bridges (38). To investigate this, we simulated two variants, one in which the termini were left charged and the other in which the termini were capped by acetylating the N-terminus and amidating the C-terminus. Five billion MC steps were performed for each replica, and a replica exchange was attempted every 1000 steps.

Only the conformations at the near-physiological lowest four temperatures (275, 290, 307, and 324 K) were considered for the conformational preferences of the peptide.

Relative Free Energy. The relative free energy (ΔG) of a state with respect to the global minimum observed in a simulation was calculated using the equation

$$\Delta G = -k_B T \ln \left(\frac{p_i}{p_{\min}} \right)$$

where k_B is the Boltzmann constant, T is the temperature, and p_i and p_{\min} are the number of elements in bin i and the global minimum (most populated bin), respectively, from a simulation. The radius of gyration (R_g), which is an indicator of how far the atoms in a molecule are from its center of mass, was plotted against the root-mean-square deviation (rmsd) of the peptide from the initial extended structure. These data were then binned,

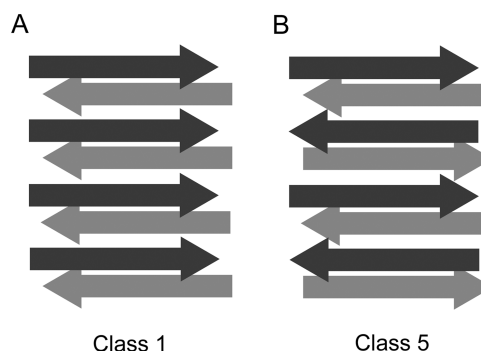


FIGURE 2: Model of class 1 and class 5 steric zippers. The orientation of a β -strand is shown as a block arrow. The first sheet is shown with black arrows and the second sheet with gray arrows.

and the ΔG for a bin with respect to the global minimum from the simulation was calculated using the equation given above.

Steric Zipper Simulations. Two classes of steric zippers, the parallel class 1 and antiparallel class 5 (26), were obtained from Jean et al. (4). Each simulation box consisted of eight strands per sheet and four sheets in one explicit box of TIP3P water molecules. The class 1 zipper assembly was enclosed in a box with dimensions of 75 Å × 75 Å × 40.16 Å and the class 5 zipper in a box with dimensions of 75 Å × 75 Å × 39.07 Å. The shorter length represents the fibril axis. Using periodic boundary conditions and a constant volume, a near-infinite fibril emulated as stacked sheets was simulated. The orientation of β -strands in the wild-type simulations is shown in Figure 2. In this instance, the newer GROMACS 4.0.5 (39) was used since it scales better over a larger number of processors. The remainder of the simulation parameters were identical to those mentioned in Molecular Dynamics. Duplicate simulations of 100 ns each were performed in each case.

In silico mutations were introduced using PyMOL (40) to generate two single-mutant structures, W6A and M10A, that prevent fibril formation (4). For each class, an additional set of simulations in which all histidines were protonated to mimic pH variations was performed.

RESULTS

Simulations of the AChE helical bundle with PRAD indicate that, apart from a bit of end fraying, the four helical AChE structures retain their helicity throughout the course of the 50 ns simulations (Figure 3A and Figure S2A,B of the Supporting Information). The intermittent loss of helicity is rapidly recovered, suggesting that the complex has a high propensity to remain a helix in the complex. Furthermore, the 14-residue AChE fragment (demarcated by red horizontal lines) retains its helicity during the course of the simulation. This is also evident in the shortest AChE chain (chain I), where the C-terminal fraying encroaches into the 14-residue fragment. However, the helicity is

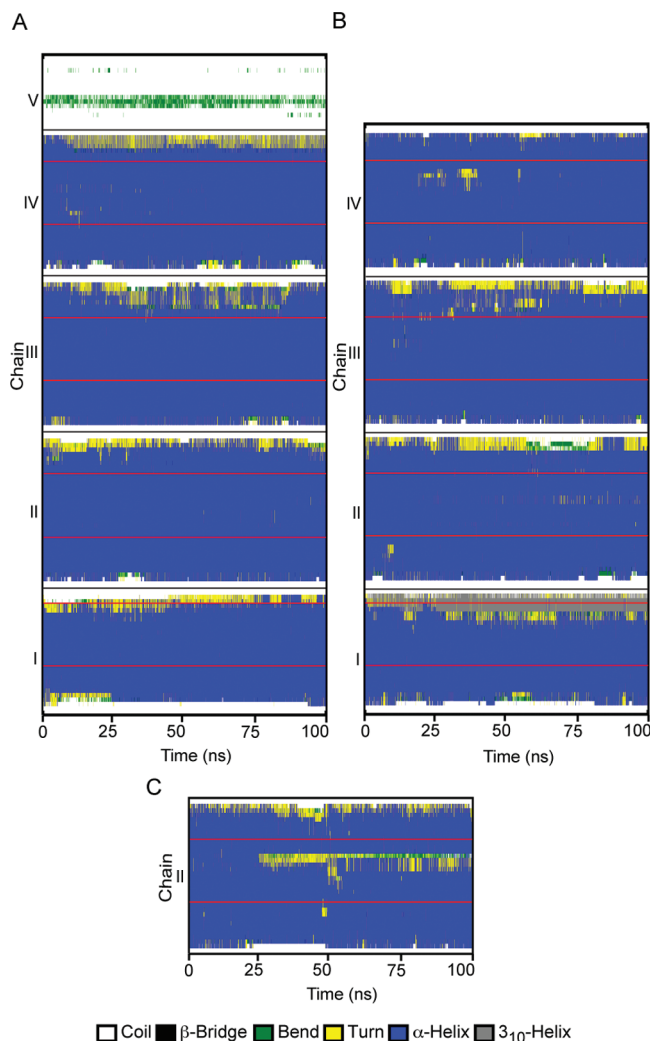


FIGURE 3: Secondary structure of the protein chains over the course of a simulation: (A) AChE–PRAD complex, (B) AChE tetramer without PRAD, and (C) AChE monomer. The N-terminus is at the bottom and the C-terminus at the top of each secondary structure plot. The AChE peptide region is demarcated with a pair of horizontal red lines.

not disrupted. $C\alpha$ distance matrices generated from the starting structure and averaged across the entire simulation trajectory indicate a consistent pattern of contacts (Figure S4 of the Supporting Information).

It has been suggested that the AChE tetramer remains intact even in the absence of the association domain (10, 41). In the second set of simulations, PRAD was removed from the structure, leaving four AChE helices. Apart from the loss of helicity near the C-terminus of truncated chain I, the helices continue to retain the helicity in the absence of PRAD (Figure 3B and Figure S2C,D of the Supporting Information), suggesting that the domain is not critical for keeping the tetrameric assembly intact and helical. However, the shorter chain I with fewer interhelix contacts exhibits signs of unfolding well into the 14-residue fragment, perhaps indicating that the regions flanking the fragment are necessary to keep the fragment predominantly helical. Furthermore, secondary structure predicted using the hidden β -propensity method for this sequence fragment showed that the C-terminal half of the peptide has a significantly stronger propensity to form β -strands (4). Loss of interhelix contacts between chains I and IV and the formation of additional contacts between chains I and III are also evident in the $C\alpha$ distance

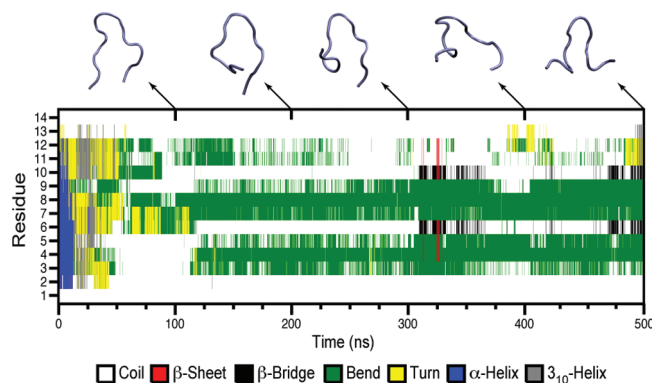


FIGURE 4: Secondary structure of the 14-residue AChE peptide as a function of time. The simulation was started from a helical conformation. Snapshots of the peptide structure at 100, 200, 300, 400, and 500 ns are also shown.

matrices for these simulations (Figure S5 of the Supporting Information).

Next, the stability of an individual helix was studied via extraction of one of the chains (chain II with 34 residues). Surprisingly, in all three simulations, much of the peptide remains helical (Figure 3C and Figure S2E,F of the Supporting Information). However, the loss of helicity in two regions is appreciable. First, the 14-residue peptide fragment (demarcated by the red horizontal lines) starts unfolding, right in the middle in two of three simulations, from which it never recovers. Despite this, large sections of the fragment still retain helicity. Second, the loss of helicity is much more prominent near the C-terminal region in contrast with the tetrameric assembly, suggesting that the interhelix contacts are essential for keeping it intact.

Finally, the 14-residue fragment was excised from a helix and studied via three extended MD simulations (500, 300, and 300 ns). The helix rapidly falls apart and in all cases in <40 ns (Figure 4 and Figure S3A,B of the Supporting Information). The unfolding is driven by the C-terminal half of the peptide, which happens within a few nanoseconds, while the N-terminal half appears to retain helicity for a longer period of time. Some fibrillogenic peptides were shown to adopt a β -hairpin conformation when individual copies were simulated in water (13). However, our simulations do not show such a behavior for the AChE peptide. The rather divergent secondary structure plots and corresponding free energy plots, derived from the radius of gyration (R_g) and root-mean-square deviation (rmsd) with respect to the starting structure (Figure S6 of the Supporting Information), of the three simulations indicate that the peptide is likely to be an unstructured random coil on its own in solution.

To further investigate the conformational space explored by the 14-residue fragment, we performed REMC folding (from an extended structure) and unfolding (from a helical structure) simulations in implicit solvent. The trajectories for the four lowest temperatures (275, 290, 307, and 324 K) were clustered (42), and the free energy plots were derived using two parameters: the radius of gyration (R_g) and the root-mean-square deviation (rmsd) with respect to the starting structure. The dominant clusters of the uncapped folding simulations were predominantly hairpinlike conformations and were markedly different from the capped simulations which showed no conformational preference. In the absence of explicit polar solvent molecules, salt bridges tend to be overstabilized (38). In this instance, in uncapped simulations, the charged termini are attracted to each other and tend to result in hairpins. In spite

of extensive sampling, simulations of the peptide with neutral capped termini failed to converge. This would suggest that the hairpinlike structure could be an artifact. To confirm this, the central structure of the best cluster of each of the uncapped simulations was subsequently simulated using molecular dynamics in explicit TIP3P solvent employing the same all atom OPLS force field. In explicit solvent, the hairpinlike starting structure rapidly falls apart and forms random coils but failed to converge to a distinct conformation.

Two steric zipper models, class 1 and class 5, were simulated to study the preferred mode of association of the AChE peptide fragment. In class 1 zippers, parallel β -sheets make up each layer (Figure 2A) while class 5 zippers have an antiparallel arrangement of strands in each layer (Figure 2B). A long fibril was simulated using a periodic boundary by setting an appropriate box size along the fibril axis. Large scale disorder, both intra- and intersheet, is observed in the class 1 assembly (Figure 5 and Figure S7 of the Supporting Information), while the class 5 assembly retained much of the secondary structure at the end of two 100 ns simulations (Figure 5 and Figure S7 of the Supporting Information). While water penetration along the fibril ends is observable in both classes, this is more detrimental in the class 1 assembly. Water penetrates deep into the layers, contributing to the observed disorder. In the mutant, W6A and M10A, simulations of class 1 fibrils, disorder, water penetration, and loss of secondary structure were observed (Figure 5 and Figure S7 of the Supporting Information). Class 5 fibrils, however, behave differently. In the M10A mutant, the secondary structure is largely retained, though disruption is observed near the site of the mutation (Figure 5 and Figure S7 of the Supporting Information). However, in the W6A mutant, the effect is more drastic. While the secondary structure is retained, the sheets buckled in or out, resulting in nonuniform sheet separation (Figure 5 and Figure S7 of the Supporting Information). In the class 5 steric zipper, the methionine and tryptophan of adjacent sheets are in the proximity of each other. The interaction of the methionine sulfur atom with the tryptophan ring could contribute to sheet and strand stability (43). Mutating either of these residues destabilizes the assembly. The instability of the mutant sheet assemblies may indicate their inability to form an intact fibril in the first place, as observed in experiments (4). Thus, the side chain packing and contacts these residues make are necessary for both strand association and sheet stacking. pH can influence the assembly and stability of fibrils (38). In this instance, the influence of pH was tested by protonating histidines in the AChE peptide. In both class 1 and class 5 fibrils, this resulted in massive disruption of the simulated assembly (Figure 5 and Figure S7 of the Supporting Information), indicating that histidines are unprotonated in the fibril.

DISCUSSION

In fibrils, peptides adopt conformations and secondary structure that are distinct from those of their native state. The pathway of this conformational transition is a subject of intense research. Model peptides and coarse-grained systems have been used to study peptide oligomerization (44–50). This study shows that, depending on local conditions, the peptide is capable of existing in at least three states: α -helix, random coil, and β -strand. This is a property shared by many fibrillogenic peptides (12, 13, 51). Computational and experimental studies have shown that peptides like Alzheimer's β -amyloid (12) and H1 peptide from prion

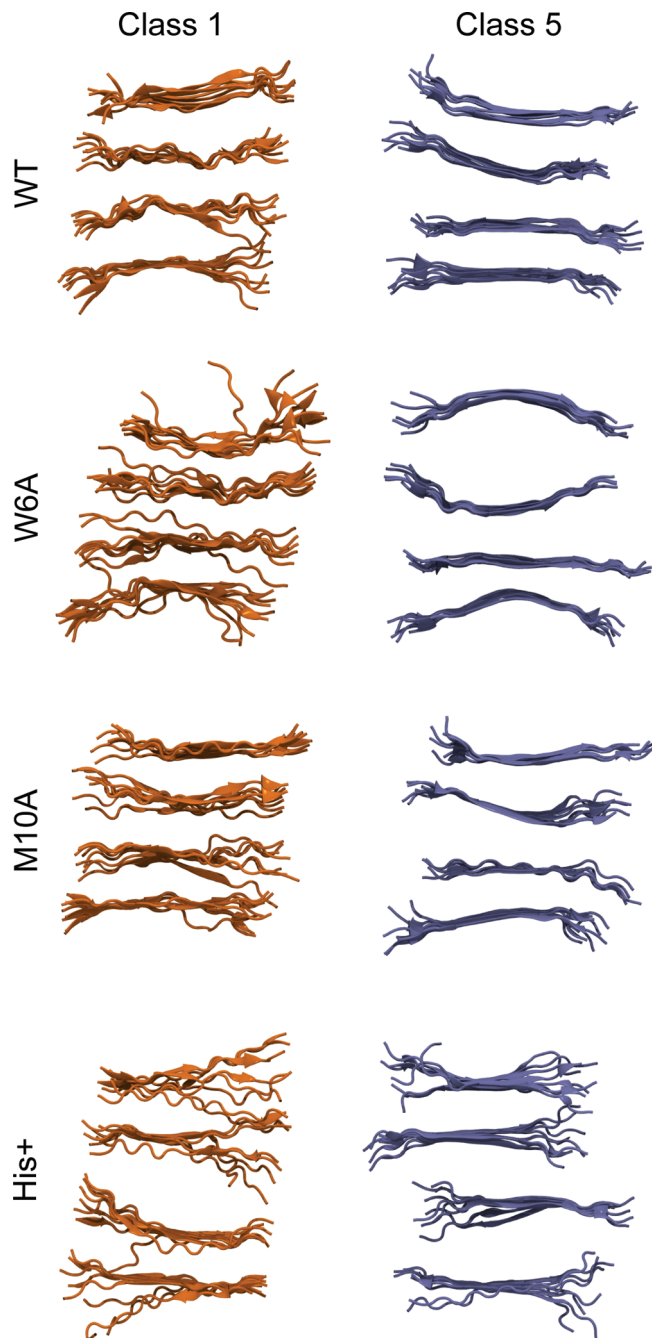


FIGURE 5: Conformation of class 1 and class 5 AChE zipper assemblies at the end of 100 ns simulations.

protein (52) exist in a multitude of states undergoing an α -helix to β -strand transition during fibrillogenesis.

In the enzymatic α -helical state, the simulation results indicate that the inter helix contact patterns (Figures S4 and S5 of the Supporting Information) are similar, irrespective of whether PRAD is present. This is in agreement with experimental studies that showed that the C-terminal region assembles as a stable tetramer even in the absence of PRAD (41). A 40-residue region encompassing the 34-residue monomer has been shown to have a helical secondary structure by using conformation-sensitive monoclonal antibodies (11). This appears to be the case in the simulations as well, though there are signs of unfolding within the 14-residue AChE peptide region. It is not surprising that the AChE peptide in isolation loses its helicity rapidly. The Zimm–Bragg helix–coil transition theory suggests that short helices tend

to be thermodynamically unstable in water and likely to unfold (53). In this instance, a multitude of techniques, MD and REMC, with explicit/implicit treatment of solvent failed to produce any distinct structure or set of structures consistent with the idea that fibrillogenic peptides could remain largely unstructured until they aggregate (51).

Aggregation typically occurs over longer time scales (25). Hence, unsurprisingly, multiple copies of AChE placed in solution did not aggregate, presumably reflecting the sampling problem. Seeding is a key step in fibril formation. Achieving this in all-atom, explicit solvent simulations mimicking physiological conditions still remains a challenging problem.

Fibrils have been broadly categorized as steric zippers depending on how protein side chains, strands, and sheets are packed (26). Performing simulations to self-assemble these zippers is a challenging task. This study considered two viable zipper models, class 1 and class 5, for the AChE peptide and compared their structural integrity. AChE peptides appear to favor the antiparallel class 5 steric zippers which affords better side chain packing and backbone hydrogen bonds that stabilize the assembly.

Determining structure from sequence has been employed in protein structure prediction, notably in the Rosetta algorithm (54), by using an assortment of known structures of similar fragments. A BLAST (55) search of the PDB (56) using the AChE sequence found numerous partial matches. The top 10 are listed in Table T1 of the Supporting Information. Cytochrome P450 and Fab appear to have residues that are similar to the AChE peptide in the N-terminal and C-terminal regions, respectively. While the cytochrome P450 residues appear to prefer a helical structure, the Fab region favors an extended conformation. This could perhaps explain why the C-terminal region unravels first in the AChE peptide. Thus, this may be a general trait of fibrillogenic peptides, the ability to morph and assemble into a nonbiologically native state.

CONCLUSION

In summary, long molecular dynamics and replica exchange Monte Carlo simulations suggest that the AChE peptide remains helical in the tetramerization complex and when part of a longer helical peptide but is largely unstructured in solution under normal physiological conditions. We remain cautious in our interpretation as the question of whether current force fields can accurately reproduce the folding landscape of small peptides is currently an area of intense investigation (57–59). Although it is known that short isolated fragments of α -helical regions tend not to form stable α -helices in solution (53), the current model for formation of amyloid-like fibrils from the AChE peptide is based upon the peptide adopting a conformation that self-assembles (4). Presumably, it is the latter aspect that distinguishes fibrillogenic peptides from nonfibrillogenic peptides. We have demonstrated here how the presence of neighboring peptides both contiguous with the segment of interest and noncovalent can influence the conformational preference of the AChE peptide. Simulations of model steric zipper assembly support the idea that the AChE fibrils could consist of antiparallel β -sheets most likely arranged as a class 5 zipper. Taken together, our results support the view that fibril formation is sensitive to specific sequences. That sensitivity arises from packing requirements within the fibril. Although we have not been able to observe fibril formation directly, a prerequisite would be that the AChE peptide, which is helical within the full-length protein, could fall out of helicity

once cleaved away. From our results presented above, that is clearly possible. The central property of a fibrillogenic fragment is that its conformational preference can be altered by the local environment (31). Simulations performed in this study show that the AChE peptide is capable of existing in a helical state in the enzyme, as a random coil in solution, and as stable antiparallel β -sheet assemblies. The data here should be useful in hierarchical models in which the longer time scale event associated with fibril formation can start to be addressed.

ACKNOWLEDGMENT

Computations were performed on the clusters of the UK National Grid Service, Oxford Supercomputing Centre, and the National Service for Computational Chemistry Software. We thank our colleagues from the laboratories of David Vaux and Susan Greenfield and Jakob and Martin Ulmschneider for helpful discussions. We thank Chiu Fan Lee for providing an initial set of coordinates for the steric zipper models.

SUPPORTING INFORMATION AVAILABLE

Sequence alignment and blast search results of the AChE peptide, secondary structure plots and contact matrices of repeat simulations, and free energy contour maps from MD simulations. This material is available free of charge via the Internet at <http://pubs.acs.org>.

REFERENCES

1. Silman, I., and Sussman, J. L. (2005) Acetylcholinesterase: 'Classical' and 'non-classical' functions and pharmacology. *Curr. Opin. Pharmacol.* 5, 293–302.
2. Greenfield, S. A., Zimmermann, M., and Bond, C. E. (2008) Non-hydrolytic functions of acetylcholinesterase. The significance of C-terminal peptides. *FEBS J.* 275, 604–611.
3. Cottingham, M. G., Hollinshead, M. S., and Vaux, D. J. T. (2002) Amyloid fibril formation by a synthetic peptide from a region of human acetylcholinesterase that is homologous to the Alzheimer's amyloid- β peptide. *Biochemistry* 41, 13539–13547.
4. Jean, L., Lee, C. F., Shaw, M., and Vaux, D. J. (2008) Structural elements regulating amyloidogenesis: A cholinesterase model system. *PLoS One* 3, No. e1834.
5. Greenfield, S. A., Day, T., Mann, E. O., and Bermudez, I. (2004) A novel peptide modulates $\alpha 7$ nicotinic receptor responses: Implications for a possible trophic-toxic mechanism within the brain. *J. Neurochem.* 90, 325–331.
6. Greenfield, S. (2005) A peptide derived from acetylcholinesterase is a pivotal signalling molecule in neurodegeneration. *Chem.-Biol. Interact.* 157–158, 211–218.
7. Zbarsky, V., Thomas, J., and Greenfield, S. (2004) Bioactivity of a peptide derived from acetylcholinesterase: Involvement of an ivermectin-sensitive site on the $\alpha 7$ nicotinic receptor. *Neurobiol. Dis.* 16, 283–289.
8. Greenfield, S., and Vaux, D. J. (2002) Parkinson's disease, Alzheimer's disease and motor neurone disease: Identifying a common mechanism. *Neuroscience* 113, 485–492.
9. Jean, L., Thomas, B., Tahiri-Alaoui, A., Shaw, M., and Vaux, D. J. (2007) Heterologous amyloid seeding: Revisiting the role of acetylcholinesterase in Alzheimer's disease. *PLoS One* 2, No. e652.
10. Dvir, H., Harel, M., Bon, S., Liu, W.-Q., Vidal, M., Garbay, C., Sussman, J. L., Massoulié, J., and Silman, I. (2004) The synaptic acetylcholinesterase tetramer assembles around a polyproline II helix. *EMBO J.* 23, 4394–4405.
11. Cottingham, M. G., Voskuil, J. L. A., and Vaux, D. J. T. (2003) The intact human acetylcholinesterase C-terminal oligomerization domain is α -helical in situ and in isolation, but a shorter fragment forms β -sheet-rich amyloid fibrils and protofibrillar oligomers. *Biochemistry* 42, 10863–10873.
12. Ikebe, J., Kamiya, N., Ito, J.-I., Shindo, H., and Higo, J. (2007) Simulation study on the disordered state of an Alzheimer's β amyloid peptide A β (12–36) in water consisting of random-structural, β -structural, and helical clusters. *Protein Sci.* 16, 1596–1608.

13. Daidone, I., Simona, F., Roccatano, D., Broglia, R. A., Tiana, G., Colombo, G., and Di Nola, A. (2004) β -Hairpin conformation of fibrillogenic peptides: Structure and α - β transition mechanism revealed by molecular dynamics simulations. *Proteins* 57, 198–204.
14. Shirts, M., and Pande, V. (2000) Screen savers of the world unite! *Science* 290, 1903–1904.
15. Dill, K. A., Ozkan, S. B., Shell, M. S., and Weikl, T. R. (2008) The protein folding problem. *Annu. Rev. Biophys.* 37, 289–316.
16. Sugita, Y., and Okamoto, Y. (1999) Replica-exchange molecular dynamics method for protein folding. *Chem. Phys. Lett.* 314, 141–151.
17. Roux, B., and Simonson, T. (1999) Implicit solvent models. *Biophys. Chem.* 78, 1–20.
18. Ho, B. K., and Dill, K. A. (2006) Folding very short peptides using molecular dynamics. *PLoS Comput. Biol.* 2, No. e27.
19. Ulmschneider, J. P., and Jorgensen, W. L. (2003) Monte Carlo backbone sampling for polypeptides with variable bond angles and dihedral angles using concerted rotations and a Gaussian bias. *J. Chem. Phys.* 118, 4261–4271.
20. Ulmschneider, J. P., and Jorgensen, W. L. (2004) Polypeptide folding using Monte Carlo sampling, concerted rotation, and continuum solvation. *J. Am. Chem. Soc.* 126, 1849–1857.
21. Ulmschneider, J. P., and Ulmschneider, M. B. (2007) Folding simulations of the transmembrane helix of virus protein U in an implicit membrane model. *J. Chem. Theory Comput.* 3, 2335–2346.
22. Ulmschneider, J. P., Ulmschneider, M. B., and Di Nola, A. (2006) Monte Carlo vs molecular dynamics for all-atom polypeptide folding simulations. *J. Phys. Chem. B* 110, 16733–16742.
23. Ulmschneider, J. P., Ulmschneider, M. B., and Di Nola, A. (2007) Monte Carlo folding of trans-membrane helical peptides in an implicit generalized Born membrane. *Proteins* 69, 297–308.
24. Ulmschneider, M. B., and Ulmschneider, J. P. (2008) Membrane adsorption, folding, insertion and translocation of synthetic trans-membrane peptides. *Mol. Membr. Biol.* 25, 245–257.
25. Kayed, R., Head, E., Thompson, J. L., McIntire, T. M., Milton, S. C., Cotman, C. W., and Glabe, C. G. (2003) Common structure of soluble amyloid oligomers implies common mechanism of pathogenesis. *Science* 300, 486–489.
26. Sawaya, M. R., Sambashivan, S., Nelson, R., Ivanova, M. I., Sievers, S. A., Apostol, M. I., Thompson, M. J., Balbirnie, M., Wiltzius, J. J. W., McFarlane, H. T., Madsen, A. Ø., Riekel, C., and Eisenberg, D. (2007) Atomic structures of amyloid cross- β spines reveal varied steric zippers. *Nature* 447, 453–457.
27. Van der Spoel, D., Lindahl, E., Hess, B., Groenhof, G., Mark, A. E., and Berendsen, H. J. C. (2005) GROMACS: Fast, flexible, and free. *J. Comput. Chem.* 26, 1701–1718.
28. Lindahl, E., Hess, B., and van der Spoel, D. (2001) GROMACS 3.0: A package for molecular simulation and trajectory analysis. *J. Mol. Model.* 7, 306–317.
29. Jorgensen, W. L., and Tirado-Rives, J. (1988) The OPLS [optimized potentials for liquid simulations] potential functions for proteins, energy minimizations for crystals of cyclic peptides and crambin. *J. Am. Chem. Soc.* 110, 1657–1666.
30. Kaminski, G. A., Friesner, R. A., Tirado-Rives, J., and Jorgensen, W. L. (2001) Evaluation and reparametrization of the OPLS-AA force field for proteins via comparison with accurate quantum chemical calculations on peptides. *J. Phys. Chem. B* 105, 6474–6487.
31. Sgourakis, N. G., Yan, Y., McCallum, S. A., Wang, C., and Garcia, A. E. (2007) The Alzheimer's peptides A β 40 and 42 adopt distinct conformations in water: A combined MD/NMR study. *J. Mol. Biol.* 368, 1448–1457.
32. Jorgensen, W. L., Chandrasekhar, J., Madura, J. D., Impey, R. W., and Klein, M. L. (1983) Comparison of simple potential functions for simulating liquid water. *J. Chem. Phys.* 79, 926–935.
33. Van Gunsteren, W. F., and Berendsen, H. J. C. (1988) A leap-frog algorithm for stochastic dynamics. *Mol. Simul.* 1, 173–185.
34. Berendsen, H. J. C., Postma, J. P. M., van Gunsteren, W. F., DiNola, A., and Haak, J. R. (1984) Molecular dynamics with coupling to an external bath. *J. Chem. Phys.* 81, 3684–3690.
35. Hess, B., Bekker, H., Berendsen, H. J. C., and Fraaije, J. G. E. M. (1997) LINCS: A linear constraint solver for molecular simulations. *J. Comput. Chem.* 18, 1463–1472.
36. Kabsch, W., and Sander, C. (1983) Dictionary of protein secondary structure: Pattern recognition of hydrogen-bonded and geometrical features. *Biopolymers* 22, 2577–2637.
37. Qiu, D., Shenkin, P. S., Hollinger, F. P., and Still, W. C. (1997) The GB/SA Continuum Model for Solvation. A Fast Analytical Method for the Calculation of Approximate Born Radii. *J. Phys. Chem. A* 101, 3005–3014.
38. Geney, R., Layten, M., Gomperts, R., Hornak, V., and Simmerling, C. (2006) Investigation of salt bridge stability in a generalized born solvent model. *J. Chem. Theory Comput.* 2, 115–127.
39. Hess, B., Kutzner, C., van der Spoel, D., and Lindahl, E. (2008) GROMACS 4: Algorithms for highly efficient, load-balanced, and scalable molecular simulation. *J. Chem. Theory Comput.* 4, 435–447.
40. DeLano, W. L. (2002) The PyMOL Molecular Graphics System, DeLano Scientific, Palo Alto, CA.
41. Bon, S., and Massoulié, J. (1997) Quaternary associations of acetylcholinesterase. I. Oligomeric associations of T subunits with and without the amino-terminal domain of the collagen tail. *J. Biol. Chem.* 272, 3007–3015.
42. Daura, X., Gademann, K., Jaun, B., Seebach, D., van Gunsteren, W. F., and Mark, A. E. (1999) Peptide Folding: When Simulation Meets Experiment. *Angew. Chem., Int. Ed.* 38, 236–240.
43. Tatko, C. D., and Waters, M. L. (2004) Investigation of the nature of the methionine- π interaction in β -hairpin peptide model systems. *Protein Sci.* 13, 2515–2522.
44. Buchete, N.-V., Tycko, R., and Hummer, G. (2005) Molecular dynamics simulations of Alzheimer's β -amyloid protofilaments. *J. Mol. Biol.* 353, 804–821.
45. Lee, C. F., Loken, J., Jean, L., and Vaux, D. J. (2009) Elongation dynamics of amyloid fibrils: A rugged energy landscape picture. *Phys. Rev. E: Stat., Nonlinear, Soft Matter Phys.* 80, 041906.
46. Nguyen, H. D., and Hall, C. K. (2004) Molecular dynamics simulations of spontaneous fibril formation by random-coil peptides. *Proc. Natl. Acad. Sci. U.S.A.* 101, 16180–16185.
47. Nguyen, H. D., and Hall, C. K. (2006) Spontaneous fibril formation by polyanilines: Discontinuous molecular dynamics simulations. *J. Am. Chem. Soc.* 128, 1890–1901.
48. Urbanc, B., Cruz, L., Ding, F., Sammond, D., Khare, S., Buldyrev, S. V., Stanley, H. E., and Dokholyan, N. V. (2004) Molecular dynamics simulation of amyloid β dimer formation. *Biophys. J.* 87, 2310–2321.
49. Urbanc, B., Cruz, L., Yun, S., Buldyrev, S. V., Bitan, G., Teplow, D. B., and Stanley, H. E. (2004) In silico study of amyloid β -protein folding and oligomerization. *Proc. Natl. Acad. Sci. U.S.A.* 101, 17345–17350.
50. Ma, B., and Nussinov, R. (2002) Molecular dynamics simulations of alanine rich β -sheet oligomers: Insight into amyloid formation. *Protein Sci.* 11, 2335–2350.
51. Andreola, A., Bellotti, V., Giorgetti, S., Mangione, P., Obici, L., Stoppini, M., Torres, J., Monzani, E., Merlini, G., and Sunde, M. (2003) Conformational switching and fibrillogenesis in the amyloidogenic fragment of apolipoprotein a-I. *J. Biol. Chem.* 278, 2444–2451.
52. Daidone, I., Amadei, A., and Di Nola, A. (2005) Thermodynamic and kinetic characterization of a β -hairpin peptide in solution: An extended phase space sampling by molecular dynamics simulations in explicit water. *Proteins* 59, 510–518.
53. Zimm, B. H., and Bragg, J. K. (1959) Theory of the Phase Transition between Helix and Random Coil in Polypeptide Chains. *J. Chem. Phys.* 31, 526–535.
54. Das, R., and Baker, D. (2008) Macromolecular modeling with rosetta. *Annu. Rev. Biochem.* 77, 363–382.
55. Altschul, S. F., Gish, W., Miller, W., Myers, E. W., and Lipman, D. J. (1990) Basic local alignment search tool. *J. Mol. Biol.* 215, 403–410.
56. Berman, H. M., Westbrook, J., Feng, Z., Gilliland, G., Bhat, T. N., Weissig, H., Shindyalov, I. N., and Bourne, P. E. (2000) The Protein Data Bank. *Nucleic Acids Res.* 28, 235–242.
57. Best, R. B., Buchete, N.-V., and Hummer, G. (2008) Are current molecular dynamics force fields too helical? *Biophys. J.* 95, L07–L09.
58. Freddolino, P. L., Park, S., Roux, B., and Schulten, K. (2009) Force field bias in protein folding simulations. *Biophys. J.* 96, 3772–3780.
59. Shell, M. S., Ritterson, R., and Dill, K. A. (2008) A test on peptide stability of AMBER force fields with implicit solvation. *J. Phys. Chem. B* 112, 6878–6886.